

## Topologically Protected Transport of Cargo in a Chiral Active Fluid Aided by Odd-Viscosity-Enhanced Depletion Interactions

Qing Yang,<sup>1,2,\*</sup> Hongwei Zhu,<sup>3,4,\*</sup> Peng Liu<sup>1,2,5</sup>, Rui Liu,<sup>1</sup> Qingfan Shi,<sup>3</sup> Ke Chen,<sup>1,2,6</sup>  
Ning Zheng<sup>3,†</sup>, Fangfu Ye,<sup>1,2,5,6,7,‡</sup> and Mingcheng Yang<sup>1,2,6,§</sup>

<sup>1</sup>Beijing National Laboratory for Condensed Matter Physics and Laboratory of Soft Matter Physics, Institute of Physics, Chinese Academy of Sciences, Beijing 100190, China

<sup>2</sup>School of Physical Sciences, University of Chinese Academy of Sciences, Beijing 100049, China

<sup>3</sup>School of Physics, Beijing Institute of Technology, Beijing 100081, China

<sup>4</sup>Inner Mongolia Dynamic and Mechanical Institute, Hohhot 010010, China

<sup>5</sup>Wenzhou Institute, University of Chinese Academy of Sciences, Wenzhou, Zhejiang 325001, China

<sup>6</sup>Songshan Lake Materials Laboratory, Dongguan, Guangdong 523808, China

<sup>7</sup>Oujiang Laboratory, Wenzhou, Zhejiang 325000, China



(Received 16 December 2020; accepted 22 April 2021; published 12 May 2021)

The discovery of topological edge states that unidirectionally propagate along the boundary of system without backscattering has enabled the development of new design principles for material or information transport. Here, we show that the topological edge flow supported by the chiral active fluid composed of spinners can even robustly transport an immersed intruder with the aid of the spinner-mediated depletion interaction between the intruder and boundary. Importantly, the effective interaction significantly depends on the dissipationless odd viscosity of the chiral active fluid, which originates from the spinning-induced breaking of time-reversal and parity symmetries, rendering the transport controllable. Our findings propose a novel avenue for robust cargo transport and could open a range of new possibilities throughout biological and microfluidic systems.

DOI: [10.1103/PhysRevLett.126.198001](https://doi.org/10.1103/PhysRevLett.126.198001)

*Introduction.*—The concept of topological insulator, originally discovered in electronic quantum Hall state [1–7], has been generalized to a variety of physical systems, ranging from mesoscopic photonic materials [8–10] to macroscopic mechanical lattices [11–15], and from passive fluids [16–20] to active matters [21–24]. Thanks to nontrivial bulk band structures, topological insulator systems, being insulating in the bulk, hold topologically protected edge modes [7,10,15,20], which propagate unidirectionally along the system boundary and are immune to disorder. The edge modes thus provide robust channels for information or material transport. Because of their fundamental interest and potential application, the exploration and exploitation of topological edge states is at the forefront of condensed-matter physics.

Without exception, the one-way edge modes either directly transport the essential constituents of topologically nontrivial systems (e.g., electron or photon) [7,10] or transmit the edge excitations of the constituents (like phonon) [15,19,20]. Comparing to traditional fluid flows that can entrain immersed objects, a quite interesting question is whether or not a topological edge flow can topologically and unidirectionally transport an intruder (i.e., cargo) that itself does not support an edge mode. Fundamentally different from the entrainment of an object by the traditional fluid flow, the topological edge transport

of the intruder, if feasible, provides a robust, one-way, and local edge channel for cargo transport, immune to obstacles. However, the presence of the topological edge flow does not mean that the immersed intruder can also experience a topological edge transport. To achieve such a cargo transport, two additional conditions are required. First, the intruder needs to spontaneously and stably stay clinging to the boundary such that it can be robustly entrained by the local edge flow along the system boundary, otherwise the intruder will often locate in the bulk. Second, the intruder can be controllably released from the boundary at the expected target position, otherwise the intruder will always stay at the boundary. For topologically nontrivial systems, the two conditions seem rather unusual to be satisfied.

Here, we study the feasibility of the topologically protected edge transport of the intruder in a chiral active matter through experiment, simulation, and theory. The chiral active matter consists of a two-dimensional fluid of interacting self-spinning particles [25,26], which breaks both time-reversal and parity symmetries. Interestingly, the chiral active fluid spontaneously yields a one-way edge flow along the system boundary [25,27–29], which was proven to be topologically protected by mapping to model quantum Hamiltonians with nontrivial topology [30]. Moreover, the spinner fluid possesses a nondissipative

transport coefficient called “odd viscosity” or “Hall viscosity” [31–36], which was usually discussed in the context of quantum Hall fluids [37]. The odd viscosity arises from the breaking of time-reversal symmetry [38,39] and is related to spinner activity [31,32].

When immersing an intruder in the chiral active fluid, the spinners give rise to a depletionlike attraction between the intruder and boundary, which is inclined to push the intruder to the boundary. Importantly, the odd viscosity can significantly strengthen the effective attraction, which is tunable through the spinner activity. Thus, the present system meets all the conditions required for the topological edge transport of the intruder. Our findings constitute proof of principle that topological edge flow can robustly transport cargoes, and extend the concept of topological edge transport from the constituents of topological systems to the immersed intruders.

*Experiment.*—The experimental spinners are granular gears of external diameter  $\sigma_s$  with tilted legs [Fig. 1(a)], fabricated via a 3D printer [29]. A monolayer of spinners are put in a circular vessel of radius  $R_v \simeq 10\sigma_s$  mounted on an electromagnetic shaker, whose vertical vibration is translated into a unidirectional active rotation of the spinner [40], with the spin angular velocity  $\omega_s$ . Meanwhile, the spinner experiences stochastic motion. The interactions between the gears are short-ranged repulsive, with a large interparticle friction. This active fluid exhibits a topologically protected edge flow [30], with its direction determined by the gear rotation. It has been shown that the topological edge flow can generally occur at a boundary and is not sensitive to the boundary geometry and the system size, as long as the spinners have nonvanishing friction with the environment [30].

To study if the topological edge flow of the spinners can robustly transport an immersed intruder, we put a large smooth passive disk of diameter  $\sigma_p$  in the spinner fluid, and fix a long and thin obstacle at the vessel boundary [Fig. 1(c)]. Because of the depletionlike interaction between the intruder and boundary mediated by the spinners (depletants), which still exists in macroscopic and nonequilibrium systems [41–45], the passive intruder tends to stay at the container boundary, and then is unidirectionally entrained along the boundary by the topological edge flow, as displayed in Fig. 1(c) [40]. Strikingly, when encountering the obstacle, the intruder clings to and bypasses it without back reflection, since the obstacle can be regarded as a part of the boundary. This result clearly indicates that the intruder can indeed be robustly transported by the topological edge flow of the spinner fluid. Because the spinner edge flow is quite robust, as long as the intruder-boundary depletion attraction is sufficiently strong, a stable edge transport of the intruder will take place, insensitive to the boundary properties. Note that the depletionlike attraction is negligible in conventional molecular fluids, since the attraction range determined by the molecular size is too small.

The edge flow velocity of the spinners and the transport velocity of the intruder are quantified in Fig. 2(a). Both velocities increase with the spinner packing fraction  $\rho$  in the fluid regime, since the driving force of the edge flow, arising from the interspinner friction, increases with  $\rho$ . Moreover, because the edge flow decays quickly from the boundary and the intruder is entrained averagely by the fluid flow located around  $\sigma_p/2$  with respect to the boundary, the intruder transport velocity is smaller than the edge flow velocity of the spinner (at  $\sigma_s/2$  from the boundary).

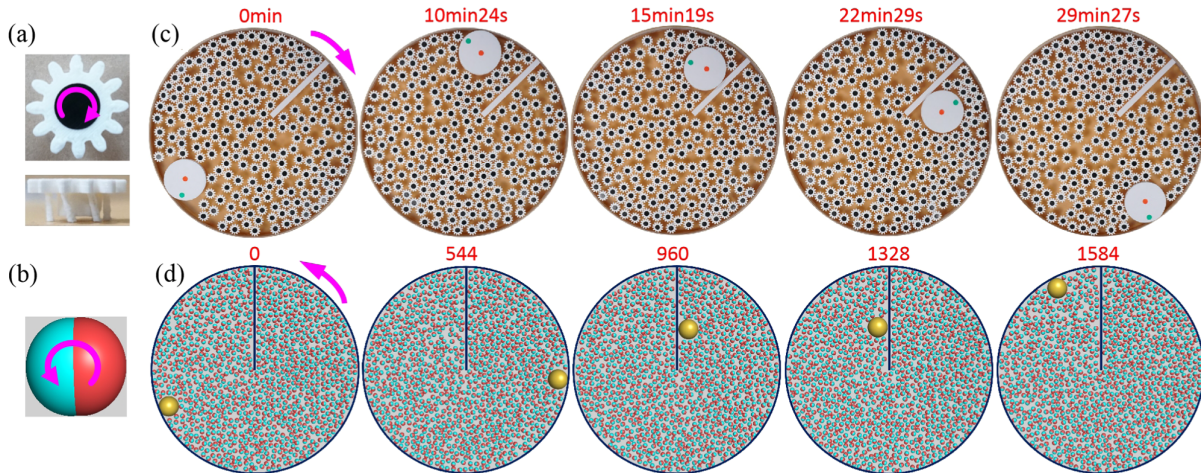


FIG. 1. (a) Top view (top) and side view (bottom) of the gearlike spinner in experiments. The arrow denotes the clockwise rotation of the spinner. (b) Sketch of the counterclockwise rotating spinner in simulations, which is intendedly represented as a Janus particle to highlight its orientation. (c) Experimental and (d) simulation snapshots of a large passive disk transported in the chiral active fluid confined by a circular boundary with a rodlike obstacle, where  $\sigma_p = 4\sigma_s$  and  $\rho = 0.6$ . In (c) and (d), the red numbers denote the experimental and the scaled simulation times, respectively, and the arrows represent the direction of the edge transport (edge flow). In the simulation  $T_d = 20$  is used.

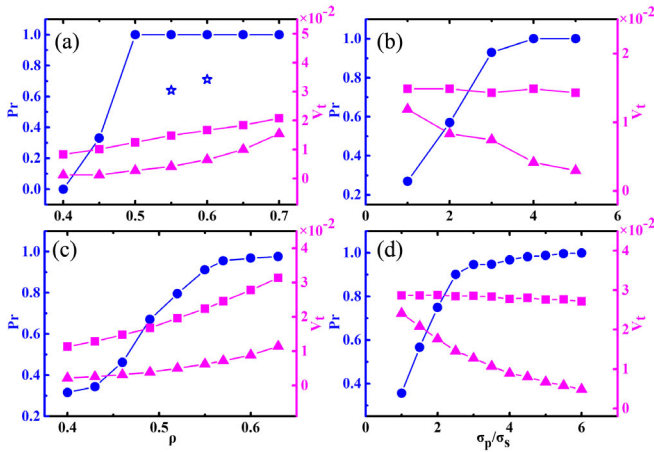


FIG. 2. Dwell probability (circle, left longitudinal axis) and transport velocity (triangle, right longitudinal axis) of the intruder as a function of the spinner packing fraction (a),(c) and the intruder size (b),(d). For comparison, the spinner edge flow velocity (square) is plotted. Here, the velocities are reduced by an isolated-spinner quantity  $\omega_s \sigma_s$  [40]. The star in (a) denotes Pr in the passive gear fluid. The data in (a),(b) and (c),(d) correspond to the experiment and simulation, respectively. In (a),(c),  $\sigma_p = 4\sigma_s$ ; and in (b),(d),  $\rho = 0.55$  for experiments and  $\rho = 0.6$  for simulations. In simulations  $T_d = 10$  is used.

We define the dwell probability of the intruder at the boundary  $Pr$  as the ratio of the intruder dwell time at the boundary to the experimental duration after the intruder first touching the boundary. The  $Pr$  increases with  $\rho$  and saturates to 1 over  $\rho = 0.5$  (i.e., stable transport) [Fig. 2(a)], meaning that the depletionlike interaction strengthens with the depletant concentration, similar to the equilibrium case [46,47]. Figure 2(b) shows that the intruder transport velocity decreases with increasing  $\sigma_p$ , as the center of larger intruder separates farther from the boundary (subject to smaller local flow). While,  $Pr$  grows with  $\sigma_p$  and approaches 1 when  $\sigma_p > 3\sigma_s$ , implying that the larger intruder suffers from the stronger depletion attraction, as the equilibrium case [46,47].

For comparison, we also measure  $Pr$  of the intruder in a fluid of passive gears with completely vertical legs. In this case, the active rotation, hence the edge flow, are absent [40]. We find for  $\rho = 0.6$  (0.55),  $Pr$  is 0.71 (0.64) [stars in Fig. 2(a)], much lower than their active counterparts ( $Pr \simeq 1$ ). So, the equilibrium depletion effect is not strong enough for a stable transport. This implies that the active spinning largely enhances the depletion attraction on the intruder, which is attributed to the odd viscosity of the spinner fluid, as will be discussed later.

*Simulation.*—In simulations, the spinner is modeled as a disk driven by a torque  $T_d$  [Fig. 1(b)]. Different spinners interact via a short-ranged repulsive potential and a tangential friction [29,40,48]; while both the wall-particle and intruder-spinner interactions are repulsive without friction. The particle dynamics evolves according to the

Langevin equation [40], with the spinner translational and rotational friction coefficients from the environment separately  $\gamma_s$  and  $\gamma_r = \frac{1}{3}\sigma_s^2\gamma_s$ , and the intruder friction coefficient taken as  $\gamma_p = \gamma_s$ . For  $T_d = 5$ , the simulation and experimental spinners have a similar Péclet number. Figure 1(d) displays typical simulation snapshots [40], reproducing the experimental observations. In simulations, we also quantify the dwell probability and transport velocity of the intruder for various  $\rho$  and  $\sigma_p$  [Figs. 2(c) and 2(d)], which well agree with the experiments. We point out that the intruders of other shapes can still exhibit similar edge transport, whose transport speeds depend on the separation between the intruder center and the boundary.

To further probe the experimentally observed increase of  $Pr$  of the intruder induced by the spinner rotation, which is critical for a stable edge transport, we perform simulations for various  $T_d$ . Figure 3(a) shows that both  $Pr$  and the intruder transport velocity increase with  $T_d$ . The stable transport ( $Pr \simeq 1$ ) can only be realized for  $T_d$  beyond a threshold, otherwise the intruder can diffuse away from the boundary, indicating that the intruder edge transport can be controlled by tuning the spinner activity. The  $T_d$  dependence of the transport velocity is directly related to the increase of the edge flow velocity with  $T_d$ ; while the dependence of  $Pr$  on  $T_d$  originates from the enhanced depletion force on the intruder due to the spinning. Figure 3(b) shows that the depletion attraction between the intruder and boundary indeed strengthens with  $T_d$ , which is obtained from independent simulations with the intruder clinging to the external wall. When the intruder-boundary effective attractive potential largely overwhelms thermal kinetic energy,  $Pr$  approaches 1. In equilibrium, the depletion interaction is proportional to the osmotic pressure contributed by small depletants [46,49]; while, in the spinner fluid, the effective attraction is determined by the radial stress on the intruder exerted by the spinners. Based on this picture, we theoretically investigate the mechanism of the spinning-enhanced depletion interaction.

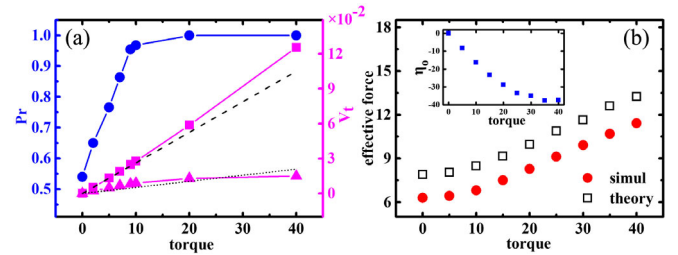


FIG. 3. (a) Edge flow velocity of the spinner (square) and transport velocity (triangle) and dwell probability (circle) of the intruder as a function of  $T_d$ . Dashed and dotted lines are separately the velocities of the spinner and the intruder, obtained from Eq. (4). (b) Effective attraction on the intruder versus  $T_d$ , obtained from simulation (circle) and theory (square). The inset plots the odd viscosity of the spinner fluid versus  $T_d$ . Here, we fix  $\rho = 0.6$  and  $\sigma_p = 4\sigma_s$ .

*Theory.*—The chiral active fluid is described by a 2D continuum hydrodynamic theory [31,32], with the incompressible condition, as used in previous work [25,28,30,32]. The hydrodynamic variables are the momentum density  $\varrho \mathbf{v}(\mathbf{r}, t)$  and the angular momentum density  $I\omega(\mathbf{r}, t)$ , with  $\varrho$  the mass density and  $I$  the moment-of-inertia density.

The conservation of momentum takes the form

$$\varrho(\partial_t + \mathbf{v} \cdot \nabla)v_i = \partial_j \sigma_{ij} - \Gamma v_i, \quad (1)$$

with  $\Gamma$  the frictional coefficient from environment, related to its single-particle counterparts by  $\Gamma = 4\gamma_s \rho / \pi \sigma_s^2$ . The stress tensor  $\sigma_{ij}$  is expressed as

$$\begin{aligned} \sigma_{ij} = & -p\delta_{ij} + \eta(\partial_i v_j + \partial_j v_i) + \epsilon_{ij}\eta_R(2\omega - \Omega) \\ & + \eta_o(\partial_i \epsilon_{jk} v_k + \epsilon_{ik} \partial_k v_j), \end{aligned} \quad (2)$$

with  $p$  the pressure,  $\epsilon_{ij}$  the Levi-Civita symbol, and  $\Omega = \hat{\mathbf{z}} \cdot (\nabla \times \mathbf{v})$  the vorticity of the flow field. In Eq. (2), the second term refers to the shear stress with  $\eta$  the shear viscosity, the third term to the antisymmetric frictional stress that couples the spin to the flow with  $\eta_R$  the rotational viscosity, and the last term to the stress contributed by the dissipationless odd viscosity  $\eta_o$ . The odd viscosity term is allowed in the chiral active fluid due to the breaking of time-reversal and parity symmetries, and its microscopic origin can be intuitively understood by comparing Figs. 4(a) and 4(b). In the presence of a

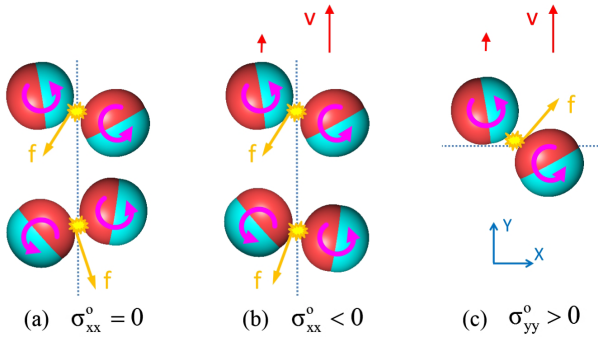


FIG. 4. Sketch of the frictional collisions between spinners separated by an imaginary plane (dashed line), illustrating the origin of the odd viscosity. The yellow arrow at one spinner surface denotes the friction exerted by the other. (a) In the absence of shear flow, the interparticle collision direction (from center to center) is uniformly distributed, so the interparticle friction averagely produces a tangential stress parallel to the plane, corresponding to the rotational viscosity term in Eq. (2), and does not contribute to normal stress. (b),(c) In the presence of a shear flow  $\partial_x v_y > 0$  (red arrow), the spinners on the right have larger upward velocity, so they are inclined to collide with their left neighbors from below, resulting in a biased collision direction. Such biased collisions contribute to a nonzero normal stress  $\sigma^o$  across the imaginary plane, which is (b) negative for a plane parallel to the flow and (c) positive for a plane perpendicular to the flow.

shear flow, the odd viscosity leads to a nonzero normal stress.

For a quantitative analysis, we obtain  $\eta = 23.5$  and  $\eta_R = 3.32$  for  $\rho = 0.6$  from independent simulations, as done in our previous work [29]. And,  $\eta_o$  can be obtained from Eq. (2) by imposing a small uniform shear on the active fluid, say  $\partial_x v_y$ , as sketched in Figs. 4(b) and 4(c) [40]. In this case, the normal stresses across the  $x$  and  $y$  planes separately read  $\sigma_{xx} = -p + \eta_o \partial_x v_y$  and  $\sigma_{yy} = -p - \eta_o \partial_x v_y$ , so that  $\eta_o = \frac{1}{2}(\sigma_{xx} - \sigma_{yy})(\partial_x v_y)^{-1}$ . Thus, the odd viscosity is computed independently [the inset of Fig. 3(b)].

The angular momentum conservation reads

$$I(\partial_t + \mathbf{v} \cdot \nabla)\omega = -\Gamma_r \omega - 2\eta_R(2\omega - \Omega) + D\nabla^2 \omega + \tau, \quad (3)$$

with  $\Gamma_r = 4\gamma_r \rho / \pi \sigma_s^2$  the rotational friction coefficient from environment and  $\tau = 4T_d \rho / \pi \sigma_s^2$  the torque density field. Here,  $D$  is the translational diffusion coefficient, negligible for the present concentration.

We first calculate the edge flow velocity of the spinners along the external boundary wall. In a polar coordinate system, the radial velocity vanishes due to symmetry. In low Reynolds number regime, the steady-state tangential velocity  $v_t(r)$  is obtained by solving Eqs. (1) and (3) with the boundary conditions  $v_t(r=0) = 0$  and  $\sigma_{\phi r}(r=R'_w) = 0$  (frictionless wall and  $R'_w = R_w - \sigma_s/2$ ) [40],

$$v_t(r) = \frac{2\eta_R \eta' \tau I_1(r/\eta')}{\eta(\Gamma_r + 4\eta_R)I_2(R'_w/\eta') + \eta_R \Gamma_r I_0(R'_w/\eta')}. \quad (4)$$

Here,  $\eta' = [(\eta_R \Gamma_r + \eta \Gamma_r + 4\eta \eta_R) / \Gamma(\Gamma_r + 4\eta_R)]^{1/2}$ , and  $I_0$ ,  $I_1$ , and  $I_2$  are the zeroth, first, and second-order Bessel functions of imaginary argument, respectively. Inserting all known quantities into Eq. (4) yields the spinner edge velocity  $v_t(R'_w)$  and the intruder transport velocity  $v_t(R_w - \sigma_p/2)$ , in good agreement with the simulations [Fig. 3(a)].

To understand the spinning-enhanced depletion force on the intruder, we notice that the intruder can be regarded as an internal boundary, so the spinner fluid spontaneously develops an edge flow around it. The steady-state tangential velocity and pressure are similarly calculated from Eqs. (1) and (3) with the boundary conditions  $v_t(r \rightarrow \infty) = 0$  and  $\sigma_{\phi r}(r=R) = 0$  [frictionless intruder,  $R = (\sigma_p + \sigma_s)/2$ , and the intruder situated at the origin of an unbounded system] [40],

$$v_t(r) = \frac{-2\eta_R \eta' \tau K_1(r/\eta')}{\eta(\Gamma_r + 4\eta_R)K_2(R/\eta') + \eta_R \Gamma_r K_0(R/\eta')}, \quad (5)$$

with  $K_0$ ,  $K_1$ , and  $K_2$  being the zeroth, first, and second-order Hankel functions of imaginary argument, respectively, and

$$p(r) = p(\infty) + \eta_o \Omega(r). \quad (6)$$

Here,  $p(\infty)$  arises as an integration constant and corresponds to the pressure at infinity due to vanishing flow at infinity. In the absence of flow, the active spinning does not contribute to normal stress, so  $p(\infty)$  can be reasonably approximated as the equilibrium value,  $p(\infty) = (4\rho k_B T / \pi \sigma_s^2) \{1 + 2\rho[(1 - 7\rho/16)/(1 - \rho)^2 - (\rho^3/16)/8(1 - \rho)^4]\}$ , obtained from a virial expansion [50].

Equations (2) and (6) yield the radial stress on the intruder

$$\sigma_{rr}(R) = -p(\infty) - 2\eta_o v_t(R)R^{-1}, \quad (7)$$

which shows the odd viscosity contributes to a spinning-dependent radial stress, enhancing the total radial stress owing to  $\eta_o v_t(R) \geq 0$ . Since both  $\eta_o$  and  $v_t(R)$  are odd functions of the spinner chirality,  $\eta_o v_t(R) \geq 0$  remains for oppositely rotating spinners. Thus, the depletionlike attraction on the intruder at the external boundary equals to  $-\sigma_{rr}(R)A_e$ , with  $A_e$  the effective cross section of the intruder colliding with the spinner, approximated as  $A_e \approx \sigma_p$ . Combining Eqs. (5) and (7) with  $\eta_o$ ,  $p(\infty)$  and  $A_e$ , the effective attraction is obtained as a function of  $T_d$  [Fig. 3(b)], consistent with the simulation. In the above calculation, we ignore the effect of the external boundary wall on the flow around the intruder, hence the stress, as the edge flow is short ranged.

**Conclusion.**—Topological edge flow and dissipationless odd viscosity are two most fascinating features of chiral active fluids composed of spinners, analogous to quantum Hall systems. We demonstrate that the combination of the two properties with the spinner-mediated depletion interaction can lead to a robust and unidirectional edge transport of immersed passive intruder, which is immune to obstacles. Remarkably, the odd viscosity significantly enhances the intruder-boundary effective attraction, which is adjustable through the spinner activity, enabling the manipulation of the intruder transport. Our work thus reveals a novel scenario of robust cargo transport, which could be relevant in biological and synthetic active systems. It remains an interesting open question whether similar transport phenomena can be observed in other types of topologically nontrivial systems.

We thank C.M. Wang for helpful discussions. We acknowledge the support of the National Natural Science Foundation of China (No. 11874397, No. 11674365, No. 11774394, No. 11974044), the Strategic Priority Research Program of Chinese Academy of Sciences (No. XDB33030300), the K.C. Wong Education Foundation, and the Youth Innovation Promotion Association of CAS (No. 2017014).

\*These authors contributed equally to this work.

†ningzheng@bit.edu.cn

‡fye@iphy.ac.cn

§mcyang@iphy.ac.cn

- [1] K. v. Klitzing, G. Dorda, and M. Pepper, *Phys. Rev. Lett.* **45**, 494 (1980).
- [2] D. J. Thouless, M. Kohmoto, M. P. Nightingale, and M. den Nijs, *Phys. Rev. Lett.* **49**, 405 (1982).
- [3] F. D. M. Haldane, *Phys. Rev. Lett.* **61**, 2015 (1988).
- [4] C. L. Kane and E. J. Mele, *Phys. Rev. Lett.* **95**, 226801 (2005).
- [5] B. A. Bernevig, T. L. Hughes, and S.-C. Zhang, *Science* **314**, 1757 (2006).
- [6] X. L. Qi and S. C. Zhang, *Rev. Mod. Phys.* **83**, 1057 (2011).
- [7] M. Z. Hasan and C. L. Kane, *Rev. Mod. Phys.* **82**, 3045 (2010).
- [8] F. D. M. Haldane and S. Raghu, *Phys. Rev. Lett.* **100**, 013904 (2008).
- [9] Z. Wang, Y. Chong, J. D. Joannopoulos, and M. Soljačić, *Nature (London)* **461**, 772 (2009).
- [10] L. Lu, J. D. Joannopoulos, and M. Soljačić, *Nat. Photonics* **8**, 821 (2014).
- [11] C. L. Kane and T. C. Lubensky, *Nat. Phys.* **10**, 39 (2014).
- [12] B. G. Chen, N. Upadhyaya, and V. Vitelli, *Proc. Natl. Acad. Sci. U.S.A.* **111**, 13004 (2014).
- [13] R. Stüsstrunk and S. D. Huber, *Science* **349**, 47 (2015).
- [14] L. M. Nash, D. Kleckner, A. Read, V. Vitelli, A. M. Turner, and W. T. M. Irvine, *Proc. Natl. Acad. Sci. U.S.A.* **112**, 14495 (2015).
- [15] X. Mao and T. C. Lubensky, *Annu. Rev. Condens. Matter Phys.* **9**, 413 (2018).
- [16] Z. Yang, F. Gao, X. Shi, X. Lin, Z. Gao, Y. Chong, and B. Zhang, *Phys. Rev. Lett.* **114**, 114301 (2015).
- [17] A. B. Khanikaev, R. Fleury, S. H. Mousavi, and A. Alu, *Nat. Commun.* **6**, 8260 (2015).
- [18] X. Ni, C. He, X. Sun, X. Liu, M. Lu, L. Feng, and Y. Chen, *New J. Phys.* **17**, 053016 (2015).
- [19] P. Delplace, J. B. Marston, and A. Venaille, *Science* **358**, 1075 (2017).
- [20] X. Zhang, M. Xiao, Y. Cheng, M.-h. Lu, and J. Christensen, *Commun. Phys.* **1**, 97 (2018).
- [21] A. Souslov, B. C. van Zuiden, D. Bartolo, and V. Vitelli, *Nat. Phys.* **13**, 1091 (2017).
- [22] S. Shankar, M. J. Bowick, and M. C. Marchetti, *Phys. Rev. X* **7**, 031039 (2017).
- [23] K. Sone and Y. Ashida, *Phys. Rev. Lett.* **123**, 205502 (2019).
- [24] A. Souslov, K. Dasbiswas, M. Fruchart, S. Vaikuntanathan, and V. Vitelli, *Phys. Rev. Lett.* **122**, 128001 (2019).
- [25] J. C. Tsai, F. Ye, J. Rodriguez, J. P. Gollub, and T. C. Lubensky, *Phys. Rev. Lett.* **94**, 214301 (2005).
- [26] N. H. P. Nguyen, D. Klotsa, M. Engel, and S. C. Glotzer, *Phys. Rev. Lett.* **112**, 075701 (2014).
- [27] B. C. Van Zuiden, J. Paulose, W. T. M. Irvine, D. Bartolo, and V. Vitelli, *Proc. Natl. Acad. Sci. U.S.A.* **113**, 12919 (2016).
- [28] X. Yang, C. Ren, K. Cheng, and H. P. Zhang, *Phys. Rev. E* **101**, 022603 (2020).
- [29] P. Liu, H. Zhu, Y. Zeng, G. Du, L. Ning, D. Wang, K. Chen, Y. Lu, N. Zheng, F. Ye, and M. Yang, *Proc. Natl. Acad. Sci. U.S.A.* **117**, 11901 (2020).
- [30] K. Dasbiswas, K. K. Mandadapu, and S. Vaikuntanathan, *Proc. Natl. Acad. Sci. U.S.A.* **115**, E9031 (2018).

- [31] D. Banerjee, A. Souslov, A. G. Abanov, and V. Vitelli, *Nat. Commun.* **8**, 1573 (2017).
- [32] V. Soni, E. S. Bililign, S. Magkiriadou, S. Sacanna, D. Bartolo, M. J. Shelley, and W. T. Irvine, *Nat. Phys.* **15**, 1188 (2019).
- [33] Z. Liao, M. Han, M. Fruchart, V. Vitelli, and S. Vaikuntanathan, *J. Chem. Phys.* **151**, 194108 (2019).
- [34] C. Hargus, K. Klymko, J. M. Epstein, and K. K. Mandadapu, *J. Chem. Phys.* **152**, 201102 (2020).
- [35] T. Markovich and T. C. Lubensky, [arXiv:2006.05662](https://arxiv.org/abs/2006.05662).
- [36] M. Han, M. Fruchart, C. Scheibner, S. Vaikuntanathan, W. Irvine, J. de Pablo, and V. Vitelli, [arXiv:2002.07679](https://arxiv.org/abs/2002.07679).
- [37] J. E. Avron, R. Seiler, and P. G. Zograf, *Phys. Rev. Lett.* **75**, 697 (1995).
- [38] J. E. Avron, *J. Stat. Phys.* **92**, 543 (1998).
- [39] S. Ganeshan and A. G. Abanov, *Phys. Rev. Fluids* **2**, 094101 (2017).
- [40] See Supplemental Material at <http://link.aps.org/supplemental/10.1103/PhysRevLett.126.198001> for additional details about experimental setup, simulation method and odd viscosity, and movies.
- [41] P. M. Reis and T. Mullin, *Phys. Rev. Lett.* **89**, 244301 (2002).
- [42] S. Aumaître, C. A. Kruehle, and I. Rehberg, *Phys. Rev. E* **64**, 041305 (2001).
- [43] P. M. Reis, G. Ehrhardt, A. Stephenson, and T. Mullin, *Europhys. Lett.* **66**, 357 (2004).
- [44] Y. Baek, A. P. Solon, X. Xu, N. Nikola, and Y. Kafri, *Phys. Rev. Lett.* **120**, 058002 (2018).
- [45] P. Liu, S. Ye, F. Ye, K. Chen, and M. Yang, *Phys. Rev. Lett.* **124**, 158001 (2020).
- [46] A. D. Dinsmore, D. T. Wong, P. Nelson, and A. G. Yodh, *Phys. Rev. Lett.* **80**, 409 (1998).
- [47] M. D. Gratale, T. Still, C. Matyas, Z. S. Davidson, S. Lobel, P. J. Collings, and A. G. Yodh, *Phys. Rev. E* **93**, 050601(R) (2016).
- [48] M. P. Allen and D. J. Tildesley, *Computer Simulation of Liquids* (Oxford University Press, New York, 2017).
- [49] S. Asakura and F. Oosawa, *J. Chem. Phys.* **22**, 1255 (1954).
- [50] S. Luding, *Phys. Rev. E* **63**, 042201 (2001).